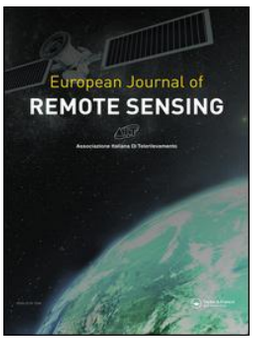

European Journal of Remote Sensing

ISSN: (Print) 2279-7254 (Online) Journal homepage: https://www.tandfonline.com/loi/tejr20

Hierarchical classification of complex landscape with VHR pan-sharpened satellite data and OBIA techniques

Marco Gianinetto, Marco Rusmini, Gabriele Candiani, Giorgio Dalla Via, Federico Frassy, Pieralberto Maianti, Andrea Marchesi, Francesco Rota Nodari & Luigi Dini

To cite this article: Marco Gianinetto, Marco Rusmini, Gabriele Candiani, Giorgio Dalla Via, Federico Frassy, Pieralberto Maianti, Andrea Marchesi, Francesco Rota Nodari & Luigi Dini (2014) Hierarchical classification of complex landscape with VHR pan-sharpened satellite data and OBIA techniques, European Journal of Remote Sensing, 47:1, 229-250, DOI: 10.5721/EuJRS20144715

To link to this article: https://doi.org/10.5721/EuJRS20144715

Published online: 17 Feb 2017.

European Journal of Remote Sensing - 2014, 47: 229-250
doi: 10.5721/EuJRS20144715
Received 19/07/2013, accepted 24/03/2014

European Journal of Remote Sensing
An official journal of the Italian Society of Remote Sensing

www.aitjournal.com

Hierarchical classification of complex landscape with VHR pan-sharpened satellite data and OBIA techniques

Marco Gianinetto[1]*, Marco Rusmini[2], Gabriele Candiani[3], Giorgio Dalla Via[1], Federico Frassy[1], Pieralberto Maianti[1], Andrea Marchesi[1], Francesco Rota Nodari[1] and Luigi Dini[4]

[1]Laboratory of Remote Sensing (L@RS), Department of Architecture, Built Environment and Construction Engineering, Politecnico di Milano, Via Ponzio 31, 20133, Milano, Italy
[2]ERM Italia S.p.A., Via San Gregorio 38, 20124, Milano, Italy
[3]Institute of Electromagnetic Sensing of Environment (IREA), Italian National Research Council (CNR), Via Bassini 15, 20133, Milano, Italy
[4]Cosmo SkyMed-CIDOT Center for the Interpretation of Earth Observation Data, Italian Space Agency, Space Geodesy Center "G.Colombo", C/da Terlecchia, c.p. 11, 75100, Matera, Italy
*Corresponding author, email address: marco.gianinetto@polimi.it

Abstract
Land-cover/land-use thematic maps are a major need in urban and country planning. This paper demonstrates the capabilities of Object Based Image Analysis in multi-scale thematic classification of a complex sub-urban landscape with simultaneous presence of agricultural, residential and industrial areas using pan-sharpened very high resolution satellite imagery. The classification process was carried out step by step through the creation of different hierarchical segmentation levels and exploiting spectral, geometric and relational features. The framework returned a detailed land-cover/land-use map with a Cohen's kappa coefficient of 0.84 and an overall accuracy of 85%.

Keywords: OBIA, hierarchical classification, land cover, VHR satellite data, pan sharpening.

Introduction
In the last few decades, remote sensing has become one of the most performing techniques for data acquisition over large areas and, nowadays, land-cover/land-use (LC/LU) thematic maps are of primary importance in all the activities related to the organization, protection and planning of our environment. In particular, urban and rural planning require an increase of detail and accuracy of the LC/LU maps.
Human interpretation still remains the main approach to information extraction from remotely sensed imagery but, even if accurate, it is highly dependent upon experts' skills [Zhang and Zhu, 2010]. Consequently, the growing demand of standardization for the processing of large dataset promoted the development of a wide range of classification algorithms and strategies, especially tuned for local mapping and urban planning [Masser, 2001; Frassy et al., 2012]. For example, the INSPIRE Directive adopted by the 27 Member States of

the European Union in 2007 established a common infrastructure for spatial information to support Community environmental policies with key components specified through technical implementing rules [European Commission, 2007; European Commission, 2008].

The on-going increase of the satellite's spatial resolution has a great impact on image classification but it does not directly implies better results [Gianinetto et al., 2004; Liu et al., 2006]. In fact, nowadays very high resolution (VHR) imaging systems are typically limited to only four spectral bands in the visible and near-infrared. Compared to most medium-resolution multispectral systems, this restricted spectral setting may lead to an overall decrease in the classification accuracy at pixel level [Aplin et al., 1999]. Things have changed with the launch of WorldView-2 (8-band) and in the next future new satellites with even higher spectral resolution are expected to be operative (e.g., WorldView-3) but, today, 4-band VHR sensors are the standard for civilian Earth Observation.

On the other hand, with sub-meter multispectral imagery the spatial extent, shape, structure and texture of land features appear fairly clear because the mixture of different land-cover classes in a single pixel is directly proportional to the pixel size. Furthermore, VHR optical images are also useful to retrieve different kind of landscape detail, such as topography-related features, which can be used as additional information during the classification process [Gianinetto, 2008, 2009].

Concerning the thematic classification of VHR data, a limitation of pixel-based approaches is the absence of semantic information on shape and relation to neighbourhood [Webb, 2003; Canty, 2009; Bhaskaran et al., 2010]. To overcome this issue, Object-Based Image Analysis (OBIA) uses segmentation to group source image pixels into self-existent and resoluble entities [Golinkoff, 2013] satisfying the Tolber's first law of Geography: "Everything is related to everything else, but near things are more related than distant things" [Tobler, 1970]. Consequently, in OBIA textural and relational information are used as additional information to the spectral properties and this approach can be extremely performing for mapping LC/LU with high and VHR data [Zhou et al., 2009].

Many authors describe OBIA studies based on single source data and basic derivatives, such as NDVI [van der Sande et al., 2003; Bock et al., 2005; Mathieu et al., 2007; Shiro, 2008; Bhaskaran et al., 2010]. Other authors combine multi-sources data as VHR imagery and LIDAR surveys [Chen et al., 2007; Pascual et al., 2008; Zhou and Troy, 2008]. Gong et al. [1992] stated that increasing the spatial resolution of image data lead to an increase in spectral variability within LC/LU classes. Furthermore, roads, bare soil, trees and grassland textural information are difficult to be fully exploited, especially in heterogeneous urban areas with a complex mosaic of buildings. Therefore, for single source data, some authors suggested to improve the classification accuracy through the introduction of first and second order textural features such as Gray Level Co-occurrence Matrices (GLCM) or Local Spatial Statistics [Rusmini et al., 2012]. Su et al. [2008] reported improvements in urban areas classification with the introduction of four GLCM textural features (i.e. homogeneity, contrast, angular second moment and entropy) and one Local Spatial Statistics feature (i.e. Moran's I), while Johansen et al. [2007] demonstrated that the introduction of GLCM textural features (i.e., homogeneity, contrast and dissimilarity) improved the mapping of forest ecosystems.

This paper describes a practical framework of OBIA for a complex landscape with a mixture of settlements, agricultural areas and industrial areas for the simultaneous classification of both urban and agricultural features into a single workflow using VHR pan-sharpened imagery.

Most of past studies distinguished between OBIA methods used for urban LC/LU mapping [Mathieu et al., 2007; Chen, 2009; Bhaskaran et al., 2010] and OBIA methods used for natural/agricultural LC/LU mapping [van der Sande et al., 2003; Bock et al., 2005; Shiro, 2008] because features are remarkably different in the two environments in terms of size, shape, and pattern. Compared to past literature, the novelty of this research is the use of OBIA for image classification of VHR satellite images in a complex scenario consisting of a mosaic of urban areas and agricultural plots. Issues concerning the different features' size was handled by using multiple hierarchical segmentation levels, while issues related to spectral mixtures among different classes were faced through the introduction of adjunctive input parameters, such as GLCM parameters, shape descriptors, spectral indexes and pan-sharpened synthetic bands.

Study area

The study area is located in the Province of Venice (Italy) and includes the villages of Dese, Praello, and the industrial area of Marcon, seven kilometres far from the Lagoon of Venice (Fig. 1). Originally dominated by agriculture, in the last decades the site has been partially urbanized and nowadays the test area consists of a complex landscape with agricultural fileds (78%) alternated to motorways, railways, and settlements (12%), and industrial sites (7%). Moreover, being close to the Venetian Lagoon, the area shows a complex system of channels and artificial water bodies (3%).

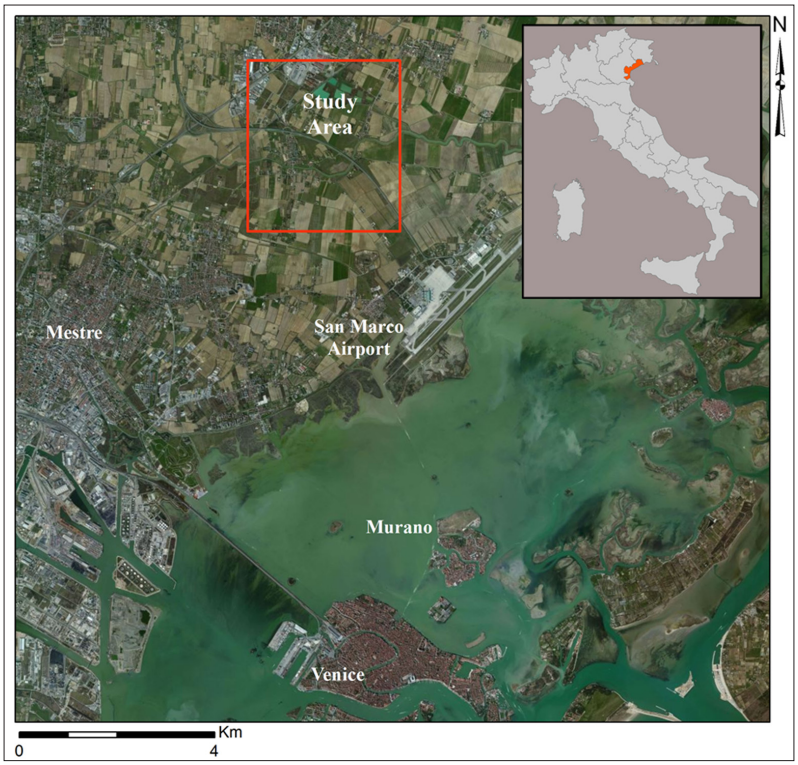

Figure 1 - Overview of the study area, Province of Venice (Italy).

Methods

Dataset

QuickBird multispectral image (panchromatic: 405-1053 nm, blue: 430-545 nm, green: 466-620 nm, red 590-710 nm and near-infrared: 715-918 nm) was collected on May 16, 2002 (spring in the experimental conditions) under clear sky conditions, with a spatial resolution of 0.64 m for the panchromatic and 2.56 m for the visible and near-infrared. The QuickBird image was taken with 11-bit radiometric resolution at a sun elevation angle of 60.9° and with off-nadir view angles of 8.63° for in-track and 9.21° for cross-track. Prior to delivery, the image was radiometrically corrected.

Data pre-processing

When using single date imagery for classification purposes, if no external training set, external reference data or spectral libraries are used, then image processing can be performed without any atmospheric correction [Song et al., 2001; Zhang and Couloigner, 2006; Del Frate et al., 2007; Pacifici et al., 2009; Zhou et al., 2009].

QuickBird data were first rectified to the world geodesic survey 1984 (WGS84) datum and the Universal Transverse Mercator (UTM) coordinate system and then pan-sharpened to increase the spatial resolution and the intra-class variability of the multispectral bands [Gong et al., 1992]. Two widely used techniques have been used: (i) Gram-Schmidt (GS) spectral sharpening [Laben, 2000] and (ii) Principal Components (PC) spectral sharpening [Shah et al., 2008]. For both methods, multispectral data have been resampled using cubic convolution and bilinear interpolation. The best dataset for thematic classification was selected by analysing the Spectral Fidelity Index [Tsai, 2004; Wang et al., 2005]. As shown in Equation 1, Q expresses the spectral fidelity and it takes into account the correlation, the average brightness and the contrast of both multispectral and pan-sharpened images [Canty, 2009]:

$$Q = \frac{\sigma_{fg}}{\sigma_f \sigma_g} \cdot \frac{2\bar{f}\,\bar{g}}{\bar{f}^2 + \bar{g}^2} \cdot \frac{2\sigma_f^2 \sigma_g^2}{\bar{f}^2 + \bar{g}^2} \quad [1]$$

where f is the multispectral image, g is the pan-sharpened image, $\bar{f}, \bar{g}$ are the mean of bands f and g, σ_f^2, (σ_g^2) are the variance of bands f and g and σ_{fg} is the covariance of bands f and g.

Table 1 - Spectral fidelity measures for the pan-sharpened QuickBird data.

Spectral bands	GS Bilinear	GS Cubic	PC Bilinear	PC Cubic
PSMS 1	0.842	0.915	0.912	0.962
PSMS 2	0.830	0.869	0.898	0.936
PSMS 3	0.814	0.810	0.879	0.893
PSMS 4	0.632	0.579	0.614	0.548
Mean	**0.779**	**0.793**	**0.826**	**0.835**

Based on results shown in Table 1, the Principal Components cubic convolution pan-sharpened image was selected as input data for thematic classification (Fig. 2).

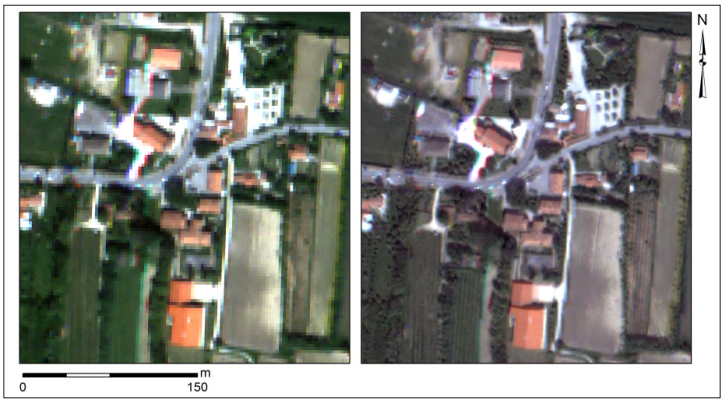

Figure 2 - Comparison between the multispectral (left) and pan-sharpened (right) images.

Image Segmentation

Image segmentation is the process of completely partitioning the scene into non-overlapping regions [Schiewe, 2002] and it is a critical step in object-based classification procedures being the selection of the input layers a major factor [Kong et al., 2006; Zhou and Troy, 2008]. An added value of OBIA is the so called hierarchical segmentation: the capability to create multiple segmentation levels connected together so that borders of broader objects are always borders of finer ones which allows to exploit semantic relations among upper and lower objects in classification procedures.

About 50% of the published papers related to OBIA used eCognition [Blaschke, 2010] for image segmentation [Aguilar et al., 2013]. Consequently, in this study eCognition was adopted. According to past studies [Johansen et al., 2007; Mathieu et al., 2007; Shiro, 2008; Su et al., 2008], image segmentation was performed on the basis of the following input layers:

a) Pan-sharpened multispectral bands (PSMS);

b) Homogeneity, contrast and dissimilarity GLCM computed with a 3x3 kernel size on the panchromatic band, as defined in Equations 2-4;

c) Normalized Difference Vegetation Index [Maselli, 2012], Normalized Difference Water Index and Spectral Shape Index [Chen et al., 2009], as defined in Equations 5-7:

$$Homogeneity = \sum_{i=1}^{N-1}\sum_{j=1}^{N-1}\frac{p(i,j)}{1+(i-j)^2} \quad [2]$$

$$Contrast = \sum_{i=1}^{N-1}\sum_{j=1}^{N-1} p(i,j)\cdot(i-j)^2 \quad [3]$$

$$Dissimilarity = \sum_{i=1}^{N-1}\sum_{j=1}^{N-1} p(i,j)\cdot|i-j| \quad [4]$$

$$NDVI = \frac{NIR - Red}{NIR + Red} \quad [5]$$

$$NDWI = \frac{Green - NIR}{Green + NIR} \quad [6]$$

$$SSI = \left| \mathrm{Re}\, d + Blue - 2 \cdot Green \right| \quad [7]$$

where i and j are either the data values in the window and the coordinates of the co-occurrence matrix space; *p(i,j)* are the normalized frequencies with which two neighbouring resolution cells separated by a fixed shift occur in the image, one with data value i and the other with data value j and N is the dimension of the co-occurrence matrix.
Five hierarchical segmentation levels have been created according to the spatial and spectral characteristics of the features to be classified, with scale factor, shape and compactness as input parameters (Tab. 2). Shape and Compactness are secondary parameters and control the shape and the dependency of objects to spectral and geometrical features [Maxwell, 2010]. The scale factor [Frauman and Wolff, 2005] was estimated through the rate of change of the local variance (Eq. 8) among a series of segmentation levels calculated with growing scale factors [Drăguţ, 2010]:

$$RoC = \left[\frac{LV - (LV - 1)}{LV - 1} \right] \cdot 100 \quad [8]$$

where *RoC* is the rate of change, *LV* is local variance of a generic level and *(LV–1)* is the local variance of the adjacent lower segmentation level.

Table 2 - Input layers and parameters used for image segmentation.

Input Layers	Level 1	Level 2	Level 3	Level 4	Level 5
PSMS 1	No	Yes	Yes	Yes	Yes
PSMS 2	No	Yes	Yes	Yes	Yes
PSMS 3	Yes	Yes	Yes	Yes	Yes
PSMS 4	Yes	Yes	Yes	Yes	Yes
Dissimilarity	Yes	No	Yes	No	No
Homogeneity	Yes	Yes	Yes	Yes	Yes
Contrast	Yes	Yes	No	No	Yes
NDVI	Yes	No	No	No	Yes
NDWI	Yes	Yes	No	No	No
SSI	Yes	No	No	No	No
Scale	48	52	107	180	440
Shape	0.2	0.4	0.3	0.4	0.7
Compactness	0.9	0.3	0.8	0.9	0.8
Starting level	Pixel Level	Level 1	Level 1	Level 1	Level 1

This method is based on the idea of local variance (LV) of the objects' heterogeneity within a scene [Woodcock and Strahler, 1987]. If the image spatial resolution is considerably finer than the objects in the scene, most of the measurements will be highly correlated with their neighbours and the LV will be small. On the other hand, if the objects approximate the size of the image resolution, the likelihood of neighbours, being similar, will decrease and the LV will rise. Based on this assumption and considering an image pixel as a segmentation object, if the objects' scale correctly represents the image features then the LV increases relatively. Figure 3 shows the results and the thresholds used for the scale factor determination.

Once defined the segmentation parameters, the upper (Level 1) and the lower (Level 5) hierarchical levels have been created and preserved for the entire process. In between these two levels, other three hierarchical levels were in turn created (Levels 2, 3 and 4) to exploit the semantic relations among the upper and lower levels and finally deleted. Table 2 shows a summary of the input parameters used.

At the end of classification process, Level 1 contained a detailed 17-class LC/LU map while Level 5 contained a broad 6 macro-classes map used to "drive" the generation of the more detailed one (Fig. 4).

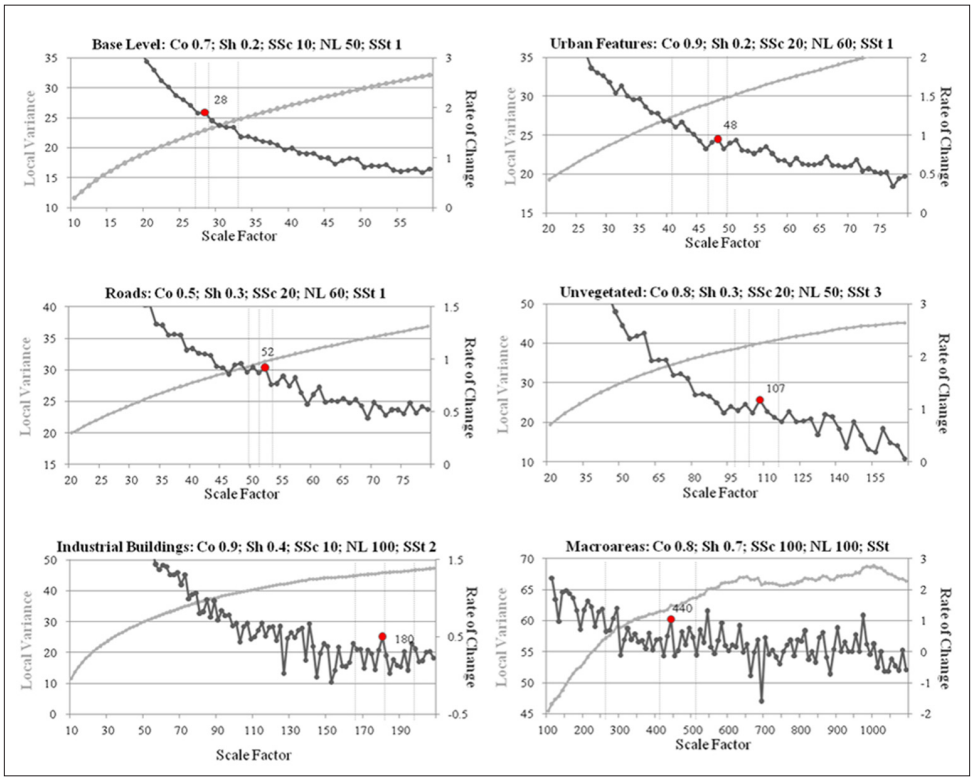

Figure 3 - Rate of change of the local variance used for the estimation of the scale factor (red dots).

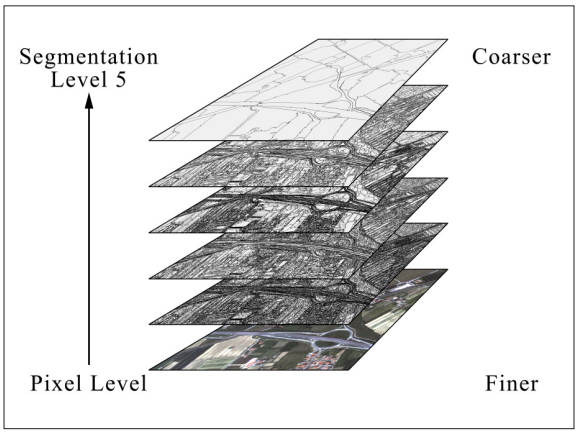

Figure 4 - Hierarchical levels created to exploit the semantic relations among the upper and lower segmentation levels.

Image Classification

OBIA allows the user to exploit spatial, geometrical and semantic relations among objects together with their spectral characteristics. To achieve a detailed LC/LU map, a broad classification into 6 macro-classes was first generated.

Classes were defined through a set of rules and organized in hierarchical groups, so that a child class inherited properties from the parent one. The classification process was carried out either by specifying thresholds for each rule (crisp classification) [Comber et al., 2012], by specifying a set of probability density functions (fuzzy classification) [HongLei et al., 2013] or through a k-Nearest Neighbour (NN) approach [Chirici et al., 2012]. Figure 5 shows the workflow.

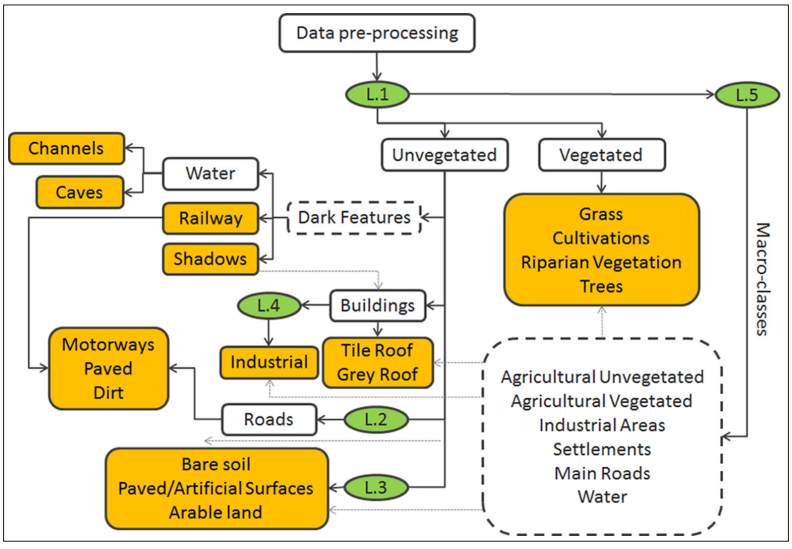

Figure 5 - Workflow of the segmentation/classification procedures (L.x means segmentation level x).

Unvegetated, vegetated, and dark features

Once created the finer segmentation level (Level 1), the first step was the partitioning into 'Vegetated' and 'Unvegetated' areas by means of an NDVI threshold: 0.4 was found suitable for the purpose. Secondly, among the 'Unvegetated' areas, the intermediate class 'Dark Features' was extracted with the following rule:

$$\begin{cases} brightness\,(PSMS3\ \&\ PSMS4) < 170 \\ brightness\,(PSMS4) < 395 \\ NDWI > 0.06 \end{cases} \quad [9]$$

This class contained shadows, dark objects (like railway) and water bodies.

Appearing as a straight line, the railway was separated using its main direction and the curvature/main length ratio, while shadows and water were differentiated through the SSI and NDWI indices. Shadows and water bodies both had high NDWI values, while SSI values were lower for the first (<274.7) and higher for the second class (>274.7), hence the two classes were differentiated through this threshold.1

Macro-classes definition

The coarser segmentation level (Level 5) was then created using a high scale parameter (440) and giving equal weight to spectral content and textural information (GLCM). With Level 5, a 6 macro-classes thematic map (Fig. 7) was generated on the basis of the following rules:

a) Shadows' number and size were assumed to be related to the number and size of buildings (Fig. 6);

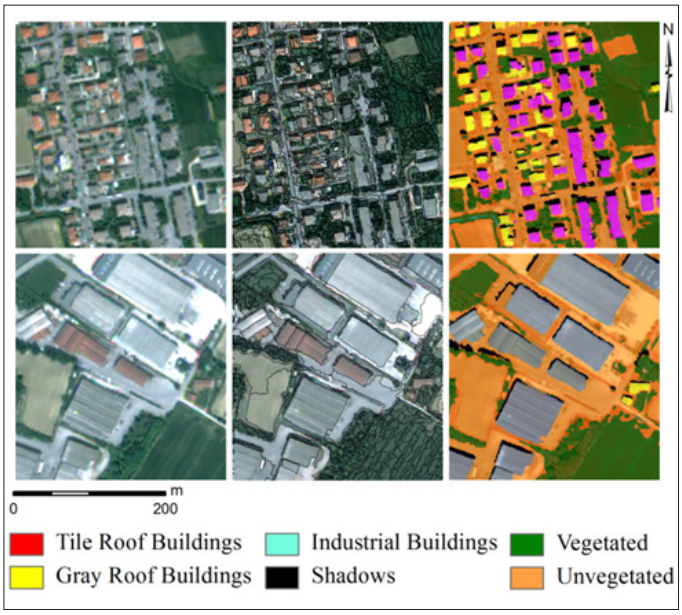

Figure 6 - Example of segmentation and classification of buildings: (top) residential buildings; (bottom) industrial buildings.

b) Agricultural areas showed a very small buildings' density, while settlements and industrial areas showed higher values;
c) Industrial areas were characterized by relatively few wide warehouses, while settlements were agglomerates of numerous small to medium residential houses;
d) Presence of water bodies or canals characterized the macro-class 'Water';
e) Vegetation density discriminated between vegetated and unvegetated agricultural areas;
f) Main roads were detected with segmentation as well as elongated narrow objects with a main direction. The classification of this layer was performed through a k-NN algorithm.

Training samples were selected on the image and membership probability functions were calculated for the following most meaningful parameters: compactness (Eq.10), asymmetry (Eq.11), mean brightness (Eq.12), mean NDVI, mean homogeneity, sub-objects shadows density (Eq.12), sub-objects shadows mean area (Eq.13) and sub-objects water density (Eq.14):

$$compactness = \frac{l_j \cdot w_j}{A_j} \quad [10]$$

$$asymmetry = \frac{\sqrt{\frac{\left(\sigma_x^2 + \sigma_y^2\right)^2 + \left(\sigma_{xy}\right)^2 - \left(\sigma_x^2 \cdot \sigma_y^2\right)}{4}}}{\sigma_x + \sigma_y} \quad [11]$$

$$\rho_j^s = \frac{N_j}{A_{sj}} \quad [12]$$

$$\overline{A}_j^s = \frac{\sum_{i=1}^{N_j} A^s}{N_j} \quad [13]$$

$$\overline{A}_j^w = \frac{\sum_{i=1}^{N_j} A^w}{N_j} \quad [14]$$

where l_j is the length of the object j, w_j is the width of the object j, A_j is the area of the object j, N_j is the number of object's shadows in the super-object j, A_{sj} is the area of the super-object j, A_s is the area of objects shadow and A_w is the area of objects water.

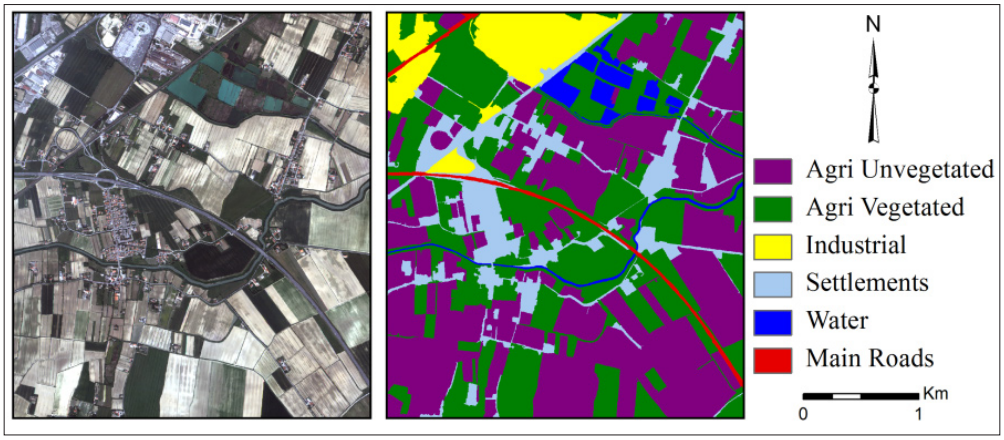

Figure 7 - Coarse 6-classes classification map.

Buildings

Two main type of buildings were present in the study area: residential houses and industrial buildings. Since the former had a mean footprint of 200 m^2 and the latter a mean footprint of 2,500 m^2, then the same segmentation level could not be used for the classification of both the categories.

Residential houses (smaller houses) were classified at the finer segmentation level (Level 1) within the already defined class 'Unvegetated', because that level well depicted residential buildings (Fig. 6). The presence of shadows was also used for the identification of buildings as in the satellite data, shadows lied to North/North-East of edifices. Consequently, the North coordinate of the shadows' centroids were calculated and residential buildings were detected among those objects with a distance ranging from -5 m to +21 m calculated between the closest shadow's centroid and the object's centroid. Because the shadows derived from the class 'Unvegetated', there was no chance of confusion with the trees' shadows.

Residential buildings were assumed to exist in the macro-classes 'Agricultural Vegetated', 'Agricultural Unvegetated', and 'Settlements'. Adjunctive thresholds were defined for the following parameters: border index (≤2), compactness (<3), length/width (≤3.9), mean NDVI (≤0.25) and rectangular fit (≤0.62).

Residential buildings were further divided into tile roofs and grey roofs based on the different response in PSMS2 and PSMS3 (Fig. 8). Seventy-four buildings were used as training samples for the calculation of the mean and standard deviation of the ratio PSMS2/PSMS3 and the threshold PSMS2/PSMS3=1.27 was used to distinguish between the two sub-classes (mean PSMS2/PSMS3=1.45 and standard deviation PSMS2/PSMS3=0.12 for grey roofs, mean PSMS2/PSMS3=1.08 and standard deviation PSMS2/PSMS3=0.13 for tile roofs).

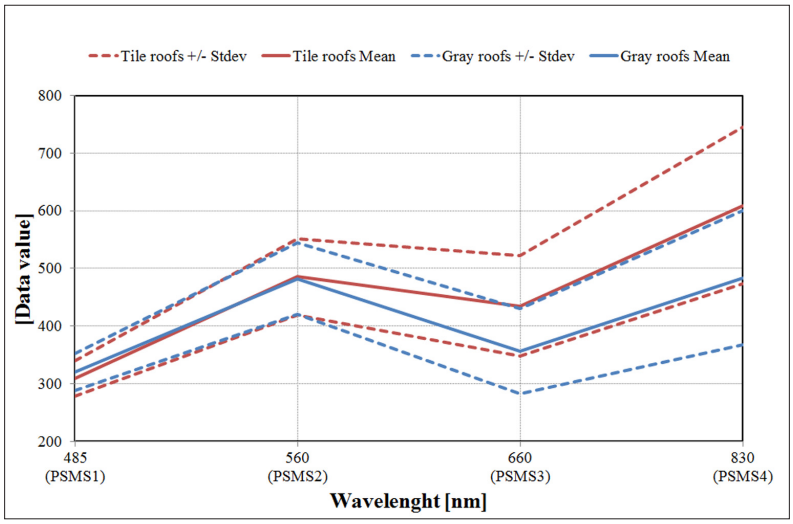

Figure 8 - Tile roofs and grey roofs reflectance behaviour. The ratio PSMS3/ PSMS2 was used for their discrimination.

Level 1 was too fine for the detection of industrial buildings, so a new coarse segmentation level (Level 4) was created (scale parameter=180) only where the macro-classes 'Industrial Areas' at Level 5 and 'Unvegetated' at Level 1 were present. This segmentation strategy allowed the extraction of the shape of wide warehouses as shown in Figure 6. The classification process exploited the same features used for residential buildings with only a little tuning on the parameter's values to consider the characteristics of the new objects.

Vegetated

Many authors suggested the use of GLCM textural features for classification of vegetation [Arivazhagan and Ganesan, 2003; Johansen et al., 2007; Murray et al., 2010; Aguilar, 2013]. In this study, according to Su et al. (2008), three different GLCM features were used: (i) contrast, (ii) homogeneity and (iii) dissimilarity. The classification of vegetated areas was carried out at the finer segmentation level (Level 1) within the already existent class 'Vegetated'. The following four sub-classes were defined: (i) forest, (ii) grass, (iii) cultivated and (iv) riparian vegetation. No ground truth was available for crop farming, so different cultivations could not be differentiated.

The first class to be extracted was 'Forest'. It has to be mentioned that QuickBird imagery was taken on April, when natural vegetation is vigorous but most of the cultivations in the study area are not yet sown (e.g., maize, paddy fields, soy), or at the very beginning of their phenological cycle (e.g, wheat, barley, beetroot) [Parati and Bonini Baraldi, 2003]. Tree canopy showed higher values of dissimilarity, contrast and NDVI with lower values of homogeneity, due to the alternation of shadowed and bright spots. The class 'Forest' was therefore defined through the following rule:

(homogeneity<0.68) AND (dissimilarity<0.55) AND (NDVI>0.40)
AND (standard deviation NIR>45)

The remaining vegetated area was assigned to the other three classes ('Grass', 'Cultivation' and 'Riparian Vegetation') by using the following spatial and relational attributes:

a) 'Grass' was defined as vegetation in residential areas, homogeneous and relatively small vegetated patches in the proximity of main roads and small spontaneous vegetation patches in unvegetated agricultural fields;

b) 'Riparian Vegetation' was defined along channels with both NDVI and homogeneity high values;

c) 'Cultivation' was defined as the remaining vegetated areas without trees with existence of super-objects 'Agricultural Vegetated'.

Road network

Once dark features, buildings, and vegetation have been classified, roads were extracted from the remaining 'Unvegetated' areas. Many authors stated that road network is unlikely to be classified through spectral properties alone [Zhang and Couloigner, 2006; Mokhtarzade and Zoej, 2007; Pacifici et al., 2009]. For example, Shackelford and Davis [2003] increased the fuzzy classification performance with the introduction of multiresolution textural features, while Chen et al. [2009] demonstrated the usefulness of spatial features in object-based classification.

In our study area, the spectral separability of roads from parking lots and grey roof buildings was extremely low. To enhance the spatial characteristics of roads, a new fine segmentation level (Level 2) was created from the remaining 'Unvegetated' areas at segmentation Level 1. The new level was similar to the previous one but the compactness parameter changed from 0.9 to 0.3 to better detect elongated objects.

The road network was extracted through spatial and relational features. In particular, the following spatial parameters were used: compactness (Ci>2.8), length/width ratio (Ri>2.4) and area index (Si>0.85), as defined in Equations 15-17:

$$C_i = \frac{l_i \cdot w_i}{P_i} \quad [15]$$

$$R_i = \frac{l_i}{w_i} \quad [16]$$

$$S_i = \frac{\sqrt{\frac{1}{4}\left(\sigma_x^2 + \sigma_y^2\right)^2 + \left(\sigma_{xy}\right)^2 - \left(\sigma_x^2 \cdot \sigma_y^2\right)}}{\sigma_x^2 + \sigma_y^2} \quad [17]$$

where l_i and w_i are length and width of object i, P_i is the number of inner pixels of object i and A_i is the area of object i.

Being roads present in all macro-classes but 'Agricultural Unvegetated', a relational rule was created to exclude their presence from such macro-class. Once extracted, the road network

could be further classified through spectral and relational features into the following three sub-classes:

a) 'Motorways': roads with existence of super-objects 'Main Roads' at segmentation Level 5;
b) 'Dirt Roads': roads with high brightness values (>300);
c) 'Paved Roads': all the remaining roads.

Figure 9 shows the vectorized road network extracted from the QuickBird imagery superimposed to the available reference data (1:5,000 Regional Technical Map). It must be observed that pathways along the channel in the South-East of the image were not recognized due to vegetation cover. On the other hand, in the North-East part of the study area the reference network of the Regional Technical Map resulted out of date when compared to the one extracted from the QuickBird images.

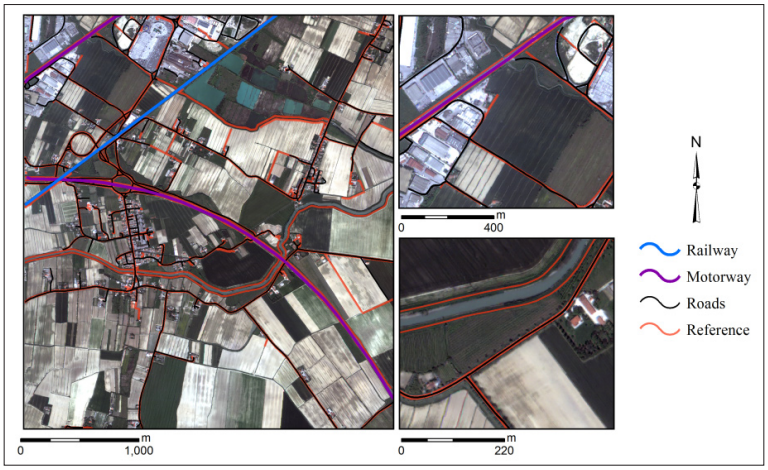

Figure 9 - Comparison of the extracted road network from QuickBird imagery with the 1:5,000 Regional Technical Map (official reference at Italian national level). Left: overall view; top right: subset on the industrial area; bottom right: subset on the channel banks.

Unvegetated

Last the classification of the remaining 'Unvegetated' areas at Level 1 into: 'Arable Land', 'Bare Soil', and 'Paved/Artificial Surfaces'.

Since unvegetated patches were wider than the objects existing in segmentation Level 1, a new medium-scale segmentation level (Level 3) was created for the remaining unclassified areas. The classification was carried out according to the following rules:

a) 'Arable Land': unvegetated areas within macro-classes 'Agricultural Unvegetated' or 'Agricultural Vegetated';
b) 'Bare Soil': bright unvegetated areas (brightness>582) within macro-classes 'Industrial' or 'Settlements';
c) 'Paved/ Artificial Surfaces': dark unvegetated areas (brightness<582).

Finally, the objects classified as 'Arable Land' but close to buildings (closer than 15 m) were post-classified as 'Bare Soil' or 'Paved/Artificial Surfaces' according to their brightness values, while objects classified as 'Arable Land' but close to caves were post-classified as 'Bare Soil' even if they appeared dark due to soil moisture.

Validation

Usually, map validation is performed through the use of pixel-based testing set. This is also true for per-pixel vs. object-based classification comparison studies [Bock et al., 2005; Mathieu et al., 2007; Chen et al., 2009; Zhou et al., 2009], although few authors suggested to carry out the accuracy assessment at object level when dealing with object-based change detection [Laliberte et al., 2004; Gamanya et al., 2009]. However, when dealing with object-based change detection.

In this study, the thematic map was validated on the basis of the 1:5,000 Regional Technical Map [Regione del Veneto, 2011] together with human interpretation of the QuickBird imagery. The error matrix was calculated using 673 per-pixel testing samples selected with an equalized random sampling scheme.

Results and discussion

Figure 10 shows the detailed hierarchical classification map consisting of 17 LC/LU.

The resulting Cohen's Kappa coefficient (κ) and Overall Accuracy (OA) were respectively 0.84 and 85%. Tables 3 and 4 show the confusion matrices, User (UA) and Producer Accuracies (PA), Commission (CE) and Omission Errors (OE) and K per class for the LC/LU classification.

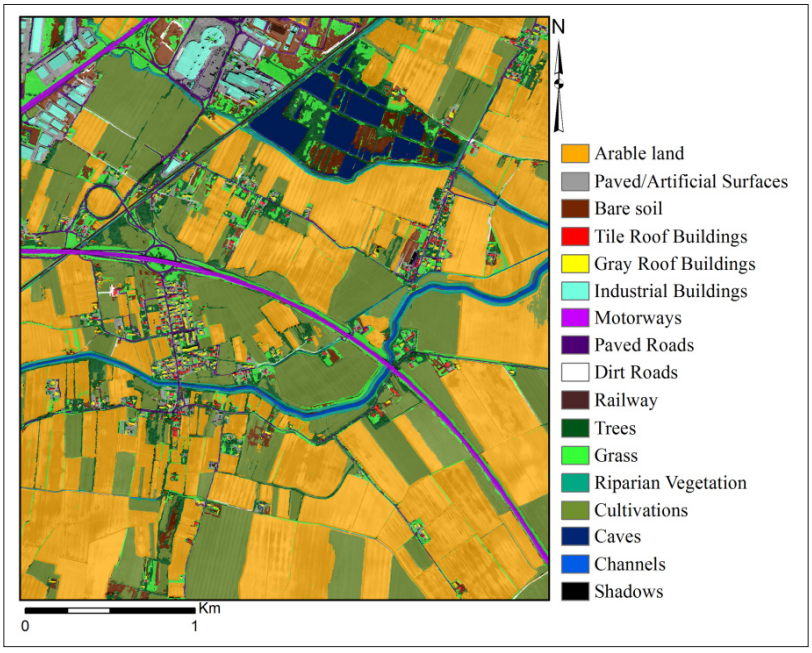

Figure 10 - Final LC/LU detailed classification map of the study area.

Table 3 - Confusion matrix of the classification map, calculated with equalized random sampled testing points.

		Ground Truth																	
	Classes	**Caves**	**Railway**	**Channels**	**Shad.**	**Tile Roof Build.**	**Gray Roof Build.**	**Indust. Build.**	**Motor.**	**Paved Roads**	**Dirt Road**	**Trees**	**Grass**	**Rip. Veg.**	**Cultiv.**	**Bare Soil**	**Paved/Art. Surf.**	**Arable Land**	**Total**
Classification	**Caves**	37	0	0	0	0	0	0	0	0	0	0	0	0	0	4	0	0	41
	Railway	0	39	0	0	0	0	0	0	0	0	0	0	0	0	0	0	0	39
	Channels	0	0	35	0	0	0	0	0	0	0	0	0	1	0	3	0	0	39
	Shadows	0	0	0	35	0	2	0	0	0	0	1	0	0	0	0	3	0	41
	Tile Roof Buildings	0	0	0	0	37	1	0	0	0	0	0	0	0	0	1	0	0	39
	Gray Roof Buildings	0	0	0	0	4	29	0	0	0	0	1	0	0	0	4	0	1	44
	Industrial Buildings	0	0	0	0	0	0	32	0	2	0	0	0	0	0	0	2	0	42
	Motorways	0	0	0	0	0	0	0	38	0	0	0	0	0	0	1	0	0	40
	Paved Roads	0	0	0	0	0	0	1	0	30	2	0	0	0	0	0	1	4	36
	Dirt Roads	0	0	0	0	0	0	0	0	2	29	0	0	0	0	8	2	0	39
	Trees	0	0	0	1	0	0	0	0	0	0	31	5	5	1	1	0	0	38
	Grass	0	0	0	0	0	0	0	0	0	0	0	39	1	2	0	0	0	41
	Riparian Vegetation	0	0	0	0	0	0	0	0	0	0	2	0	36	1	1	0	0	39
	Cultivations	0	0	0	0	0	0	0	0	0	0	0	3	1	36	0	0	0	36
	Bare Soil	0	0	0	0	0	1	0	0	0	2	0	0	0	2	26	2	6	40
	Paved/ Artificial Surfaces	0	0	0	0	0	0	4	0	1	1	0	0	0	0	1	25	4	40
	Arable Land	0	0	0	0	0	0	0	0	0	0	1	0	0	0	1	0	38	39
	Total	37	39	35	36	41	33	37	38	35	34	36	47	44	42	51	35	53	673

Overall, a high classification accuracy was obtained for most of the classes. In particular, 'Caves', 'Railways', 'Motorways' and 'Channels' had a κ=1.0. All the vegetated areas ('Trees', 'Grass', 'Riparian Vegetation' and 'Cultivations') showed homogeneous values of UA (82%<UE<86%) and PA (86%<PA<90%), with the only exclusion of the class 'Trees' that highlighted a higher CE (about 30%).

Buildings were generally misclassified with pavements and bare soil or with other building classes: tile and grey roofs did not have a sharp spectral difference, colour of bare soil was similar to tiles, while pavements showed basically the same spectral features of grey roofs. Nevertheless, all the three building classes ('Tile Roof Buildings', 'Grey Roof Buildings', and 'Industrial Buildings') showed quite good KIA per class ($0.86<\kappa<0.90$) and UA (86%<UA<90%).

On the other hand, 'Bare Soil', 'Arable Land' and 'Paved/Artificial Surfaces' showed lower UA or PA compared to the other land-cover classes. This outcome sounds reasonable

considering the similarity of their spectral signatures. In particular, 'Bare Soil' showed a very low K per class (κ=0.48). Inside unvegetated objects, this class was assumed to have high brightness values and not to be very close to buildings. Furthermore, dark areas next to caves (due to soil moisture) were forced to belong to 'Bare Soil'. On one hand, the above mentioned rules allowed the integration in the same class of areas with very different spectral signatures, but on the other hand they led to further errors in the final classification map.

Table 4 – Accuracy assessment of the classification map.

Classes	User Acc. (%)	Prod. Acc. (%)	Comm. (%)	Omiss. (%)	K per class
Caves	100.00	90.24	9.76	0.00	1.00
Railway	100.00	100.00	0.00	0.00	1.00
Channels	100.00	89.74	10.26	0.00	1.00
Shadows	97.22	85.37	14.63	2.78	0.97
Tile Roof Buildings	90.24	94.87	5.13	9.76	0.90
Grey Roof Buildings	87.88	74.36	25.64	12.12	0.87
Industrial Buildings	86.49	88.89	11.11	13.51	0.86
Motorways	100.00	97.44	2.56	0.00	1.00
Paved Roads	85.71	78.95	21.05	14.29	0.85
Dirt Road	85.29	70.73	29.27	14.71	0.84
Trees	86.11	70.45	29.55	13.89	0.85
Grass	82.98	86.00	7.14	17.02	0.82
Riparian Vegetation	81.82	90.00	10.00	18.18	0.81
Cultivations	85.71	90.00	10.00	14.29	0.85
Bare Soil	50.98	66.67	33.33	49.02	0.48
Paved/Artificial Surfaces	71.43	69.44	30.56	28.57	0.70
Arable Land	71.70	95.00	5.00	28.30	0.70

Conclusion

The limited spectral resolution of actual sub-meter imaging systems and the increasing demand of standardization for map updating makes thematic classification of complex sub-urban environments not a simple task.

In past, OBIA has been used for the classification of urban or natural/agricultural LC/LU, but not for the classification of a complex patchy landscape in the same framework. This study showed a practical application of Object-Based Image Analysis for land-cover/land-use classification using VHR pan-sharpened satellite imagery in which issues related to differences in the features' size of the natural and urban environments were handled using multiple hierarchical levels. The framework here presented may be considered as a general scheme and should be replicated in different areas with a limited tuning.

Overall, the method proposed showed an accuracy of about 85% (for both OA and κ), which is very close to other author's findings considering only the urbanized environment [Aguilar et al., 2013] with similar input data (GeoEye-1 or WorldView-2 pan-sharpened images). Moreover, the use of shadows in discriminating buildings proved to be effective in a complex sub-urban area, pushing the buildings classification accuracy near to 90%.

Acknowledgements

The study is part of the research project "Evaluation of COSMO-SkyMed performances and simulation of future ORFEO system with existing optical data" related to the integration of optical and radar VHR data for thematic classification, sponsored and funded by the Italian Space Agency (ASI) in the framework "The demonstration of the COSMO-SkyMed capabilities and exploitation for science and civilian applications".

References

Aguilar M.A., Salda M.M., Aguilar F.J. (2013) - *GeoEye-1 and WorldView-2 pan-sharpened imagery for object-based classification in urban environments*. International Journal of Remote Sensing, 34 (7): 2583-2606. doi: http://dx.doi.org/10.1080/01431161.2012.747018.

Aplin P., Atkinson P.M., Curran P.J. (1999) - *Fine Spatial Resolution Simulated Satellite Sensor Imagery for Land Cover Mapping in the United Kingdom*. Remote Sensing of Environment, 68 (3): 206-216. doi: http://dx.doi.org/10.1016/S0034-4257(98)00112-6.

Arivazhagan S., Ganesan L. (2003) - *Texture classification using wavelet transform*. Pattern Recognition Letters, 24 (9-10): 1513-1521. doi: http://dx.doi.org/10.1016/S0167-8655(02)00390-2.

Bhaskaran S., Paramananda S., Ramnarayan M. (2010) - *Per-pixel and object-oriented classification methods for mapping urban features using Ikonos satellite data*. Applied Geography, 30 (4): 650-665. doi: http://dx.doi.org/10.1016/j.apgeog.2010.01.009.

Blaschke T. (2010) - *Object Based Image Analysis for Remote Sensing*. ISPRS Journal of Photogrammetry and Remote Sensing, 65: 2-16. doi: http://dx.doi.org/10.1016/j.isprsjprs.2009.06.004.

Bock M., Xofis P., Mitchley J., Rossner G., Wissen M. (2005) - *Object-oriented methods for habitat mapping at multiple scales - Case studies from Northern Germany and Wye Downs, UK*. Journal for Nature Conservation, 13 (2-3): 75-89. doi: http://dx.doi.org/10.1016/j.jnc.2004.12.002.

Canty M.J. (2009) - *Image Analysis, Classification and Change Detection in Remote Sensing with Algorithms for ENVI/IDL, 2nd edition*, Taylor & Francis.

Chen Y., Shi P., Fung T., Wang J., Li X. (2007) - *Object-oriented classification for urban land cover mapping with ASTER imagery*. International Journal of Remote Sensing, 28 (20): 4645-4651. doi: http://dx.doi.org/10.1080/01431160500444731.

Chen Y., Su W., Li J., Sun Z. (2009) - *Hierarchical object oriented classification using very high resolution imagery and LIDAR data over urban areas*. Advances in Space Research, 43 (7): 1101-1110. doi: http://dx.doi.org/10.1016/j.asr.2008.11.008.

Chirici G., Corona P., Marchetti M., Mastronardi A., Maselli F., Bottai L., Travaglini D. (2012) - *K-NN FOREST: a software for the non-parametric prediction and mapping of environmental variables by the k-Nearest Neighbors algorithm*. European Journal of Remote Sensing, 45: 433-442. doi: http://dx.doi.org/10.5721/EuJRS20124536.

Comber A., Fisher P., Brunsdon C., Khmag A. (2012) - *Spatial analysis of remote sensing image classification accuracy*. Remote Sensing of Environment, 127: 237-246. doi: http://dx.doi.org/10.1016/j.rse.2012.09.005.

Del Frate F., Pacifici F., Schiavon G., Solimini C. (2007) - *Use of Neural Networks for Automatic Classification From High-Resolution Images*. IEEE Transactions on

Geoscience and Remote Sensing, 45 (4): 800-809. doi: http://dx.doi.org/10.1109/TGRS.2007.892009.

Drăguţ L., Tiede D., Levick S.R. (2010) - *ESP: a tool to estimate scale parameter for multiresolution image segmentation of remotely sensed data*. International Journal of Geographical Information Science, 24 (6): 859-871. doi: http://dx.doi.org/10.1080/13658810903174803.

European Commission (2007) - *Directive 2007/2/EC of the European Parliament and of the Council of 14 March 2007 establishing an Infrastructure for Spatial Information in the European Community (INSPIRE)*. Official Journal of the European Union, L 108: 1-14.

European Commission (2008) - *Commission Regulation (EC) No 1205/2008 of 3 December 2008 implementing Directive 2007/2/EC of the European Parliament and of the Council as regards metadata*. Official Journal of the European Union, L 326: 12-30.

Frassy F., Candiani G., Maianti P., Marchesi A., Rota Nodari F., Rusmini M., Albonico C., Gianinetto M. (2012) - *Airborne remote sensing for mapping asbestos roofs in Aosta Valley*. In: Proccedings of the 2012 IEEE International Geoscience and Remote Sensing Symposium (IGARSS 2012), pp. 7541-7544. doi: 10.1109/IGARSS.2012.6351886.

Frauman E., Wolff E. (2005) - *Segmentation of very high spatial resolution satellite images in urban areas for segments-based classification*. The International Archive of the Photogrammetry, Remote Sensing and Spatial Information Sciences, XXXVI (part 8/W27): 1-4.

Gamanya R., De Maeyer P., De Dapper M. (2009) - *Object-oriented change detection for the city of Harare, Zimbabwe*. Expert Systems with Applications, 36 (1): 571-588, doi: http://dx.doi.org/10.1016/j.eswa.2007.09.067.

Gianinetto M., Scaioni M., Borgogno Mondino E., Giulio Tonolo F. (2004) - *Satellite images geometric correction based on non-parametric algorithms and self-extracted GCPs*. In: Proceedings of the 2004 IEEE International Geoscience and Remote Sensing Symposium (IGARSS 2004), 6: 3755-3758, doi: http://dx.doi.org/10.1109/IGARSS.2004.1369939.

Gianinetto M. (2008) - *Automatic digital terrain model generation using Cartosat-1 stereo images*. Sensor Review, 28 (4): 299-310, doi: http://dx.doi.org/10.1108/02602280810902596.

Gianinetto M. (2009) - *Evaluation of Cartosat-1 Multi-Scale Digital Modelling Over France*. Sensors, 9: 3269-3288. doi: http://dx.doi.org/10.3390/s90503269.

Golinkoff J.S. (2013) - *Area Dependent Region Merging: A Novel, User-Customizable Method to Create Forest Stands and Strata*. European Journal of Remote Sensing, 46: 511-533. doi: http://dx.doi.org/10.5721/EuJRS20134630.

Gong P., Marceau D.J., Howarth P.J. (1992) - *A comparison of spatial feature extraction algorithms for land-use classification with SPOT HRV data*. Remote Sensing of Environment, 40 (2): 137-151. doi: http://dx.doi.org/10.1016/0034-4257(92)90011-8.

HongLei Y., JunHuan P., BaiRu X., DingXuan Z. (2013) - *Sensing Classification Using Fuzzy C-means Clustering with Spatial Constraints Based on Markov Random Field*. European Journal of Remote Sensing, 46: 305-316. doi: http://dx.doi.org/10.5721/EuJRS20134617.

Johansen K., Coops N.C., Gergel S.E., Stange Y. (2007) - *Application of high spatial resolution satellite imagery for riparian and forest ecosystem classification*. Remote Sensing of Environment, 110 (1): 29-44. doi: http://dx.doi.org/10.1016/j.rse.2007.02.014.

Kong C., Xu K., Wu C. (2006) - *Classification and Extraction of Urban Land-Use Information from High-Resolution Image Based on Object Multi-features*. Journal of China University of Geosciences, 17 (2): 151-157. doi: http://dx.doi.org/10.1016/S1002-0705(06)60021-6.

Laben C.A., Brower B.V. (2000) - *Process for enhancing the spatial resolution of multispectral imagery using pan-sharpening*. United States Patent 6011875, Eastman Kodak Company.

Laliberte A.S., Rango A., Havstad K.M., Paris J.F., Beck R.F., McNeely R., Gonzalez A.L. (2004) - *Object-oriented image analysis for mapping shrub encroachment from 1937 to 2003 in southern New Mexico*. Remote Sensing of Environment, 93 (1-2): 198-210. doi: http://dx.doi.org/10.1016/j.rse.2004.07.011.

Liu Y., Li M., Mao L., Xu F., Huang S. (2006) - *Review of remotely sensed imagery classification patterns based on object-oriented image analysis*. Chinese Geographical Science, 16 (3): 282-288. doi: http://dx.doi.org/10.1007/s11769-006-0282-0.

Maselli F. (2012) - *A method to improve the spatial features of NDVI data series*. European Journal of Remote Sensing, 45: 407-420. doi: http://dx.doi.org/10.5721/EuJRS20124534.

Masser I. (2001) - *Managing our urban future: the role of remote sensing and geographic information systems*. Habitat International, 25 (4): 503-512. doi: http://dx.doi.org/10.1016/S0197-3975(01)00021-2.

Mathieu R., Freeman C., Aryal J. (2007) - *Mapping private gardens in urban areas using object-oriented techniques and very high-resolution satellite imagery*. Landscape and Urban Planning, 81 (3): 179-192. doi: http://dx.doi.org/10.1016/j.landurbplan.2006.11.009.

Maxwell S.K. (2010) - *Generating land cover boundaries from remotely sensed data using object-based image analysis: Overview and epidemiological application*. Spatial and Spatio-temporal Epidemiology, 1: 231-237. doi: http://dx.doi.org/10.1016/j.sste.2010.09.005.

Mokhtarzade M., Zoej M.J.V. (2007) - *Road detection from high-resolution satellite images using artificial neural networks*. International Journal of Applied Earth Observation and Geoinformation, 9 (1): 32-40. doi: http://dx.doi.org/10.1016/j.jag.2006.05.001.

Murray H., Lucieer A., Williams R. (2010) - *Texture-based classification of sub-Antarctic vegetation communities on Heard Island*. International Journal of Applied Earth Observation and Geoinformation, 12 (3): 138-149. doi: http://dx.doi.org/10.1016/j.jag.2010.01.006.

Pacifici F., Chini M., Emery W.J. (2009) - *A neural network approach using multi-scale textural metrics from very high-resolution panchromatic imagery for urban land-use classification*. Remote Sensing of Environment, 113 (6): 1276-1292. doi: http://dx.doi.org/10.1016/j.rse.2009.02.014.

Parati P., Bonini Baraldi A. (2003) - *La nuova carta della copertura del suolo nel bacino scolante nella laguna di Venezia: metodologia e prima applicazione nel settore agro-ambientale*. In: Proceedings of the 7th National Conference of Environmental Agencies.

Pascual C., Garcìa-Abril A., Garcìa-Montero L.G., Martìn-Fernàndez S., Cohen W.B. (2008) - *Object-based semi-automatic approach for forest structure characterization using lidar data in heterogeneous Pinus sylvestris stands*. Forest Ecology and Management, 255 (11): 3677-3685. doi: http://dx.doi.org/10.1016/j.foreco.2008.02.055.

Regione del Veneto (2011) - *La Carta Tecnica Regionale*.

Rusmini M., Candiani G., Frassy F., Maianti P., Marchesi A., Rota Nodari F., Dini L., Gianinetto M. (2012) - *High-resolution SAR and high-resolution optical data integration for sub-urban land-cover classification*. In: Proceedings of the 2012 IEEE International Geoscience and Remote Sensing Symposium (IGARSS 2012), pp. 4986-4989. doi: http://dx.doi.org/10.1109/IGARSS.2012.6352492.

Schiewe J. (2002) - *Segmentation of high-resolution remotely sensed data concepts, applications and problems*. In: Proceedings of the Symposium on Geospatial Theory, Processing and Applications.

Shackelford A.K., Davis C.H. (2003) - *A hierarchical fuzzy classification approach for high-resolution multispectral data over urban areas*. IEEE Transactions on Geoscience and Remote Sensing, 41 (9): 1920-1932. doi: http://dx.doi.org/10.1109/TGRS.2003.814627.

Shah V.P., Younan N.H., King R.L. (2008) - *An Efficient Pan-Sharpening Method via a Combined Adaptive PCA Approach and Contourlets*. IEEE Transactions on Geoscience and Remote Sensing, 46 (5): 1323-1335. doi: http://dx.doi.org/10.1109/TGRS.2008.916211.

Shiro O. (2008) - *Land cover classification based on image objects for high resolution satellite image*. Southeast Asian Studies, 46 (4): 578-592.

Song C., Woodcock C.E., Seto K.C., Lenney M.P., Macomber S.A. (2001) - *Classification and Change Detection Using Landsat TM Data: When and How to Correct Atmospheric Effects?* Remote Sensing of Environment, 75 (2): 230-244. doi: http://dx.doi.org/10.1016/S0034-4257(00)00169-3.

Su W., Li J., Chen Y., Liu Z., Zhang J., Low T.M., Suppiah I., Hashim S.A.M. (2008) - *Textural and local spatial statistics for the object-oriented classification of urban areas using high resolution imagery*. International Journal of Remote Sensing, 29 (11): 3105-3117. doi: http://dx.doi.org/10.1080/01431160701469016.

Tobler W. (1970) - *A computer movie simulating urban growth in the Detroit region*. Economic Geography, 46 (2): 234-240. doi: http://dx.doi.org/10.2307/143141.

Tsai V.J.D. (2004) - *Evaluation of multiresolution image fusion algorithms*. In: Proceedings of the 2004 IEEE International Geoscience and Remote Sensing Symposium, 1: 621-624. doi: http://dx.doi.org/10.1109/IGARSS.2004.1369104.

van der Sande C.J., de Jong S.M., de Roo A.P.J. (2003) - *A segmentation and classification approach of IKONOS-2 imagery for land cover mapping to assist flood risk and flood damage assessment*. International Journal of Applied Earth Observation and Geoinformation, 4 (3): 217-229. doi: http://dx.doi.org/10.1016/S0303-2434(03)00003-5.

Wang Z., Bovik A.C., Simoncelli E.P. (2005) - *Structural Approaches to Image Quality Assessment*. Handbook of Image and Video Processing, 2nd edition, Burlington: Academic Press, pp. 961-974. doi: http://dx.doi.org/10.1016/B978-012119792-6/50119-4.

Webb, A.R. (2003) - *Statistical Pattern Recognition, 2nd edition*. Malvern, John Wiley & Sons.

Woodcock C.E., Strahler A.H. (1987) - *The factor of scale in remote sensing*. Remote Sensing of Environment, 21 (3): 311-332. doi: http://dx.doi.org/10.1016/0034-4257(87)90015-0.

Zhang Q., Couloigner I. (2006) - *Benefit of the angular texture signature for the separation of parking lots and roads on high resolution multi-spectral imagery*. Pattern Recognition Letters, 27 (9): 937-946. doi: http://dx.doi.org/10.1016/j.patrec.2005.12.003.

Zhang R., Zhu D. (2010) - *Study of land cover classification based on knowledge rules using high-resolution remote sensing images*. Expert Systems with Applications, 38 (4): 3647-3652. doi: http://dx.doi.org/10.1016/j.eswa.2010.09.019.

Zhou W., Huang G., Troy A., Cadenasso M.L. (2009) - *Object-based land cover classification of shaded areas in high spatial resolution imagery of urban areas: A comparison study*. Remote Sensing of Environment, 113 (8): 1769-1777. doi: http://dx.doi.org/10.1016/j.rse.2009.04.007.

Zhou W., Troy A. (2008) - *An object-oriented approach for analysing and characterizing urban landscape at the parcel level*. International Journal of Remote Sensing, 29 (11): 3119-3135. doi: http://dx.doi.org/10.1080/01431160701469065.